Aerosol and Air Quality Research, 13: 122–136, 2013

ISSN: 1680-8584 print / 2071-1409 online
doi: 10.4209/aaqr.2012.07.0180

Numerical Simulation of the Acenaphthylene Compound in an Atmospheric Plasma Reactor to Treat Cooking Fumes

Hung-Chang Chang[1], Lien-Te Hsieh[1,2*]

[1] *Department of Environmental Engineering and Science, National Pingtung University of Science and Technology, No. 1, Shuefu Road, Neipu, Pingtung 91201, Taiwan*
[2] *Emerging Compounds Research Center (ECOREC), National Pingtung University of Science and Technology, No. 1, Shuefu Road, Neipu, Pingtung 91201, Pingtung, Taiwan*

ABSTRACT

Acenaphthylene (chemical formula of $C_{12}H_8$, Acpy), also known as cyclopenta[de]naphthalene, is a polycyclic aromatic hydrocarbon (PAH) with 3 aromatic rings. The Acpy compound is a PAH on the Environmental Protection Agency's (EPA's) priority pollutant list. This study presents a simulation of an atmospheric plasma reactor (APR) using a method based on computational fluid dynamics (CFD). A commercial CFD tool was used to solve mass, momentum, and energy equations. The commercial FLUENT code was then used to simulate the Acpy compound using a 3D APR to treat the cooking fume exhaust emitted from a restaurant kitchen. The simulations in this study adopted the APR size and operating parameters from a self-designed atmospheric plasma reactor in a previous study (NSC95-2221-E020-021). An in-house reduced chemical mechanism was coupled with the CFD code for improved computational runtime. The reactivity of the system was considered with the RNG *k-ε* turbulence model and the classical Eddy Dissipation Concept combustion model. The simulation results were compared with the experimental temperature measurement and the removal efficiency of Acpy. The simulated average removal efficiency of Acpy was 61.3%.

***Keywords*:** Atmospheric Plasma; Oil fume; Acenaphthylene; CFD; Air toxic.

INTRODUCTION

Polycyclic aromatic hydrocarbons (PAHs) are organic pollutants widely distributed in the environment (Yang *et al.*, 1998; Li *et al.*, 2003; Lai *et al.*, 2010; Wu *et al.*, 2010; Bari *et al.*, 2011; Masih *et al.*, 2012). As a class, PAHs are widely produced by natural sources, such as forest fires and volcanoes, and from humanmade sources, including the burning of wood in homes, cooking fume, automobile and truck emissions, tobacco smoke, and the production of coal tar and coal tar products (ATSDR, 1990; Li *et al.*, 2003; Chang *et al.*, 2011; Tsai *et al.*, 2011; Liu *et al.*, 2012). Acenaphthylene, also known as cyclopenta[de]naphthalene, is a polycyclic aromatic hydrocarbon (PAH) with 3 aromatic rings. The United States Environmental Protection Agency (U.S. EPA) has ranked acenaphthylene the 16 priority air pollutant among polycyclic aromatic hydrocarbons (U.S. EPA, 1990). Therefore, the emission of acenaphthylene from cooking behaviour/activity on both air qualities and health issues is of critical importance.

A number of PAHs cause tumors in laboratory animals that are exposed to PAHs through their food, from breathing contaminated air, and when a PAH is applied to the skin. A study on the effects of Acpy on kidney, liver, blood, the reproductive system, and the lungs was conducted by oral subchronic toxicity tests on animals. After 40 d of continuous oral Acpy administration at a dosage of 0.6 g/d, the kidney function of small rats was affected by changes in distal blood (Knobloch *et al.*, 1969). The lung function of large rats was affected after taking 176 mg/kg/d for 2 months (Rotenberg and Mashbits, 1965). Oral toxicity tests conducted for 90 d showed a correlation between the mortality increase of female rats and the dose of Acpy, after orally administering male and female rats with 100, 200, or 400 mg/kg of Acpy each day. Other effects included the volume ratio decrease of hemes and corpuscles, the decrease in soterocytes (male) and leukocytes (female), increase in liver quantity, hypertrophy of hepatocytes, kidney disease, and other relevant pathological changes. The administration of Acpy also reduced ovary quality, decreased the activity of ovaries and wombs, and resulted in atretic corpora lutea (U.S. EPA, 1989). The erythrocyte quantity of male rats and the liver quality of female rats both increased. In addition, female rats exhibited hypertrophy of hepatocytes and other

* Corresponding author. Tel.: 886-8-774-0521;
Fax: 886-8-774-0256
E-mail address: Lthsieh@mail.npust.edu.tw

relevant pathological changes when the dose was 200 mg/kg/d. The results of Acpy oral acute toxicity testing on animals showed that the LD_{50} (median lethal dose) of large rats is 3 g/kg, and that of small rats is 1.76–2.2 g/kg (Rotenberg and Mashbits, 1965; Knobloch *et al.*, 1969). However, toxicity data indicate absorption, and data from structurally related PAHs (primarily benzo[a]pyrene) suggest that acenaphthylene is absorbed readily from the gastrointestinal tract, lungs, and skin (U.S. EPA, 1991).

The application of plasma technology in handling environmental pollutants primarily involves pollutants in the solid, liquid, and gaseous phase (Hsieh *et al.*, 1998; Moustakasa *et al.*, 2005; Magureanu *et al.*, 2010). With its high-energy gas molecules, plasma can decompose tenacious, toxic molecules and harmful organic pollutants, and react with chemical compounds such as MTBE, BTEX, and other PAHs in automobile exhaust. The advantages of plasma-decomposing toxic substances at high temperature can decrease the emissions concentration of organic compounds. However, plasma technology requires high electricity consumption during operation, thus increasing its cost. Few studies have used an atmospheric pressure plasma reactor to manage cooking fumes because of the difficulty in sampling and limits of obtaining test data (Chang *et al.*, 2011). Therefore, there is a lack of understanding regarding the actual burning conditions inside a plasma reactor when using the plasma technology to treat PAHs produced during the cooking process.

In recent years, computational fluid dynamics (CFD) is widely applied to the design of various types of engine combustors, refrigeration units, and air conditioning systems. This technique is also useful for predicting the diffusion of air and water pollutants. It is widely applied in academia and is a useful tool for industrial solutions to solve engineering problems. Many reports show that the joint application of process simulation and CFD is a helpful tool in the design and optimization of complex and innovative concepts in chemical engineering. Miltner *et al.* (2007) showed that process simulation and CFD using validated models with a sound physical basis can significantly reduce the development costs and the time-to-market of innovative chemical engineering concepts.

The numerical investigation of the corona plasma region in negative wire-to-duct corona discharge and a novel computation method calculating the plasma region thickness was presented with the plasma region model (Kim *et al.*, 2010). The proposed method consists of a state-of-the-art tool employing the CFD technique to improve indoor pollution and ventilation methods. The proposed method focuses on the optimum sizing and sitting of ventilation schemes and the provision of practical suggestions as a part of an indoor pollution management system (Panagopoulos *et al.*, 2011).

This study investigates the combustion in a plasma reactor used to treat Acpy emission from the cooking process by applying the CFD method. With the appropriate calculation models, the CFD results can be used to optimize both the plasma reactor geometry and the combustion parameters regarding the improvement of efficiency and the decomposition of PAH emissions in existing systems. Environmental engineers are typically confronted with 2 difficulties. The first is the simulation of a plasma combustion system using CFD modeling, which remains a challenging domain. The second is the relatively little progress, until recently, in the application of plasma technology to treat PAH emissions. The conceptual framework and working methods of treating the Acpy compound in an atmospheric plasma reactor remain unclear. Therefore, this study uses the numerical value simulation methods to discuss reactions by applying CFD numerical simulation, and determines the temperature of gas, the flow field and rate, and the Acpy removal efficiency of the plasma system. The solution proposed in this paper is to adopt simplified plasma torch calculations instead of detailed, complex calculations because plasma torch calculations can be generated rapidly and provide information on the removal efficiency of air toxins. This rapid assessment allows immediate modification of the APCD operation system in situ. In the future, these results can assist engineers in improving plasma systems or achieve energy savings during experimental plasma reactor operation.

METHODS

Fig. 1 shows the simulation process. The simulations in this study adopted the atmospheric plasma reactor size and operating parameters from the self-designed atmospheric plasma reactor (APR) in our previous study (Hsieh, 2007; Chang *et al.*, 2011). Table 1 shows the system parameters for simulation. Fig. 2 shows the full-scale reactor. The parameter setting value was based on practical experimental data. We discuss the distributed concentration in the flow field of the reactor and the removal efficiency of Acpy compounds. The results can serve as a reference for decision-making in engineering applications.

Mesh Independent Study

A mesh was generated using the commercial grid-generation tool GAMBIT. The 3D geometry was meshed using the mesh generator GAMBIT 2.4.6 (GAMBIT, 2007). Fig. 3 shows the 3D meshed model. The mesh was a quadrilateral mesh. To seek an appropriate grid system, this study tests and compares 3 different grid systems of 493,204, 980,000, and 3,460,000 elements. Table 2 shows the 3 grid systems and the distributions of temperature. The outlet temperature discrepancies are small. Therefore, this study adopts the grid system of 493,204 elements. Fig. 4 shows the grid point distribution (XX plane) for treating Acpy using an atmospheric plasma reactor.

Atmospheric Plasma Reactor Material Boundary Conditions

The simulations in this study adopted the following boundary settings:

(1) Inlet: Initial calculation was conducted to simulate the process of the Acpy compounds of fugitive cooking fumes entering the torch reaction area under atmospheric pressure. The boundary conditions of the velocity inlet were obtained here. The inlet velocity was 6.23 m/s.

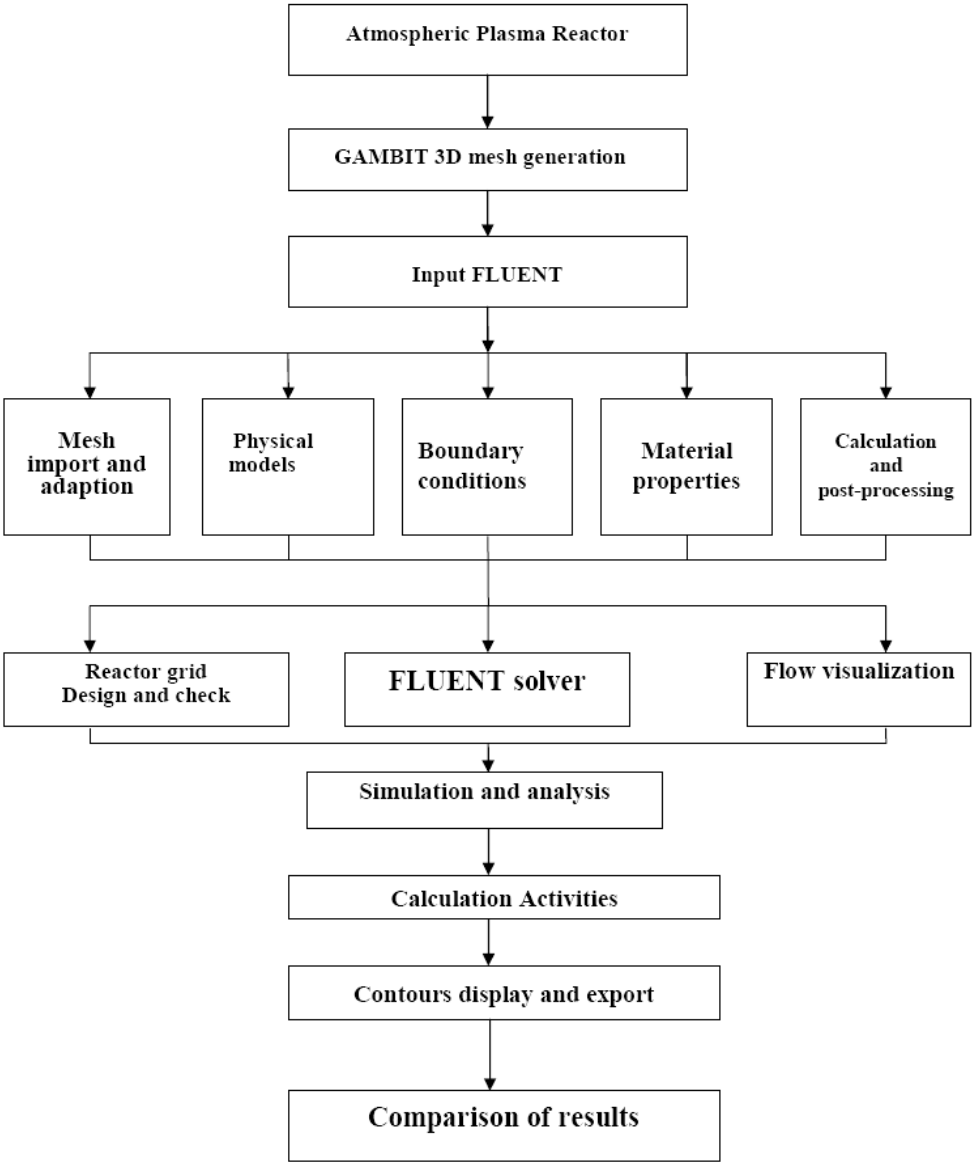

Fig. 1. Simulation process.

Table 1. System Parameters for simulation.

Parameters in Computational Fluid Dynamics	
Method	Finite Volume Method
Model	RNG *k-ε* Eddy-Dissipation Concept
Solution Method	SIMPLE
Grid	conformal
Boundary condition	inlet: velocity inlet outlet: pressure outlet Wall: stainless steel

(2) Outlet: At the outlet, the process of cooking fumes entering the airspace after passing through the torch reaction area under atmospheric pressure plasma was simulated, and the pressure outlet was applied. The outlet pressure was 1 atm.

(3) The duct vent was composed of stainless steel. Therefore, "stainless steel" was chosen as the fluent parameter, and the pipe thickness was set to 3 mm.

Numerical Method

To predict the outlet temperature and mass fraction of Acpy in the previous models, the commercial software ANSYS FLUENT 12.1 was used to solve the governing equations and the associated boundary conditions. In the software, the momentum, the energy, the species transport with the Eddy Dissipation Concept (EDC) for turbulent combustion was used. First-order upwind discretization was used for both momentum and energy equations with the semi-implicit method for pressure-linked solutions (SIMPLE) algorithm for pressure-velocity coupling. Although a second-order scheme would yield better accuracy, it is not explored because of computational time constraints. The resulting solver is based on the finite-volume method and employs a pressure-based solver with double precision. When the relative residues of all physical and chemical scales were smaller than 10^{-6}, convergence was presumed to have reached and the calculations were terminated.

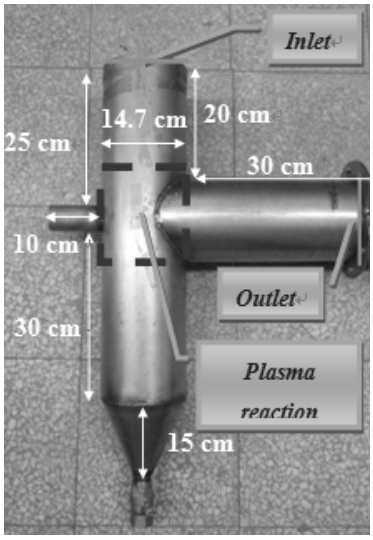

Fig. 2. A full-scale reactor

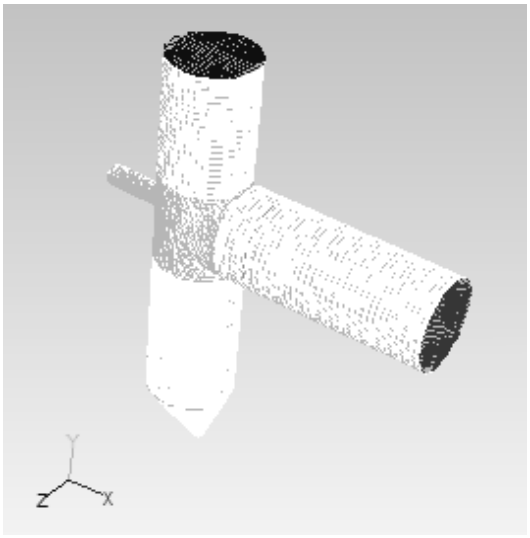

Fig. 3. 3D meshed model.

Table 2. Summary of grid independence test.

Model	Elements	Outlet temperature (K)	Deviation from model 1 (%)
Model-1	493,204	300.07181	0.000
Model-2	980,000	300.07779	0.002
Model-3	3,460,000	300.09329	0.005

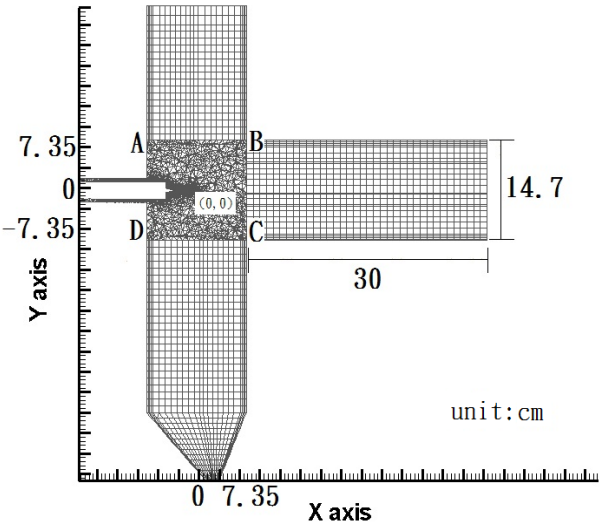

Fig. 4. A description of grid relating to the atmospheric plasma reactor. (XY profile).

RESULTS AND DISCUSSION

This study simulates the inlet of the plasma reactor as the initial operation setting level based on the concentration of experimental data (Li *et al.*, 2003; Chang *et al.*, 2011). Thus, it is similar to the emission concentration of PAHs in cooking fumes. The simulated Acpy concentration is used for calculation with 2.18×10^{-9} (mass fraction). Table 3 shows the molecular structures of the species used in this study. Because the practical combustion reaction is a complex chain reaction, this study adopts the simplified chemical reactions shown in Table 4.

To define the different relative distances used in CFD simulations, Fig. 4 uses a simple diagram to represent the different target position in the plasma reactor. Assuming that a box (ABCD volume) is the main plasma reaction of activity, the shading in the rectangle (i.e., the ABCD section) designates the plasma reaction zone in the reactor. The reactant species enter the AB-section, pass through the plasma torch, and continue through the BC-section to the exit vent. We compare the simulated results with the experimental data from a real plasma reactor. The measured volume flows, temperatures, and acenaphthylene compounds in flue gas were averaged over a quasi-stationary period.

Table 3. Molecular structures of species used in the present work.

 C_5H_5 Cyclopentadienyl	 C_5H_6 Cyclopentadiene	 C_6H_5 Phenyl, Al	 C_6H_6 Benzene, A1
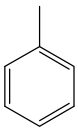 C_7H_7 Benzyl	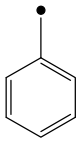 C_7H_8 Toluene	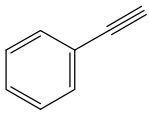 C_8H_6 Ethynylbenzene	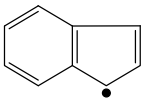 C_9H_7 1-Indenyl
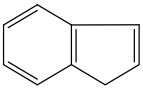 C_9H_8 Indene	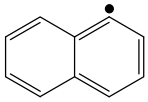 $C_{10}H_7$ 1-Naphthyl	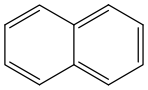 $C_{10}H_8$ Naphthalene,A2	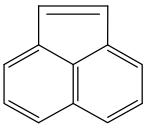 $C_{12}H_8$ Acenaphthylene, A2R5
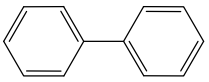 $C_{12}H_{10}$ Biphenyl, P2	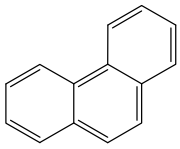 $C_{14}H_{10}$ Phenanthrene, A3	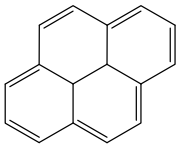 $C_{16}H_{10}$ Pyrene, A4	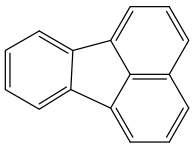 $C_{16}H_{10}$ Fluoranthene, FLTHN

Table 4. Reaction, reaction rate parameters, and references for Acenaphthylene.

R#	Reactions	A	n	*Ea*	Ref.
Selected Reactions of C_0–C_4 Species					
1	$2H + H_2 = 2H_2$	1.00E+17	–0.60	0.0	Shatalov *et al.* (2009)
2	$2H + N_2 = H_2 + N_2$	5.40E+18	–1.30	0.0	Shatalov *et al.* (2009)
3	$2H + H_2O = H_2 + H_2O$	1.00E+19	–1.00	0.0	Shatalov *et al.* (2009)
4	$OH + H_2 = H_2O + H$	1.80E+09	1.2	2370.0	Isaacson (1997)
5	$H_2 + O_2 = OH + OH$	1.20E+12	0.50	35121.0	Karkach and Osherov (1999)
6	$H + HO_2 = H_2 + O_2$	2.00E+14	0.0	1030.0	Baulch *et al.* (2005)
7	$H + HO_2 = 2OH$	3.00E+11	0.0	700.0	Baulch *et al.* (2005) × 2
8	$HO_2 + HO_2 = H_2O_2 + O_2$	1.32E+11	0.00	–820.3	Baulch *et al.* (2005)
9	$H_2O_2 + H = HO_2 + H_2$	1.21E+07	2.0	5200	Frenklach *et al.* (1995)
10	$H_2O_2 + H = OH + H_2O$	1.00E+13	0.0	3600	Frenklach *et al.* (1995)
11	$H_2O_2 + O = OH + HO_2$	9.63E+06	2.0	4000	Frenklach *et al.* (1995)
12	$CH_4 + H = CH_3 + H_2$	6.6E+08	1.62	10840.0	Smith *et al.* (1999)
13	$C_2H_2 + O_2 = HCCO + OH$	4.00E+07	1.5	30100.0	Marinov *et al.* (1998)
14	$HCCO + O_2 = CO_2 + HCO$	2.40E+11	0.0	–854.0	Marinov *et al.* (1998)
15	$C_2H_3 = C_2H_2 + H$	1.00E+15	0.0	23900.0	Wu *et al.* (2006)
16	$C_2H_4 + H = C_2H_3 + H$	1.00E+15	0.0	23900.0	Wu *et al.* (2006)
17	$C_2H_4 + OH = C_2H_3 + H_2O$	1.00E+15	0.0	23900.0	Wu *et al.* (2006)
18	$C_2H_4 + CH_3 = C_2H_3 + CH_4$	1.00E+15	0.0	23900.0	Wu *et al.* (2006)
19	$C_2H_4 + O = OH + C_2H_3$	1.00E+15	0.0	23900.0	Wu *et al.* (2006)
20	$C_3H_2 + CH_3 = C_4H_4 + H$	1.00E+13	0.0	0.0	Wang *et al.* (2007)
21	$C_3H_2 + OH = C_2H_2 + HCO$	6.80E+13	0.0	23900.0	Wu *et al.* (2006)
22	$C_3H_2 + O = C_2H_2 + CO$	6.80E+13	0.0	23900.0	Wu *et al.* (2006)
23	$C_3H_2 + H = C_3H_3$	1.00E+13	0.0	23900.0	Davis *et al.* (1999)
24	$C_3H_3 + H = C_3H_2 + H_2$	5.00E+13	0.0	1000	Wang *et al.* (2007)
25	$C_3H_3 + H_2 = C_3H_4 + H$	1.00E+15	0.0	23900.0	Wu *et al.* (2006)
26	$C_3H_3 + C_2H_2 = C_5H_5$	2.40E+11	0.00	5030	Knjazev and Slagle (2002); Slavinskaya and Frank (2009)
27	$C_3H_3 + C_2H_3 = C_5H_5 + H$	1.00E+15	0.00	1E+12	Slavinskaya and Frank (2009); p.w.

Table 4. *(continued).*

R#	Reactions	A	n	*Ea*	Ref.
28	$C_3H_3 + C_4H_4$ = Benzyl	2.00E+14	0.0	42300	Dagaut *et al.* (2002)
29	$C_3H_3 + C_3H_3 \rightarrow$ Al- + H	2.20E+33	–6.0	15940	Miller and Klippenstein (2003)
30	$C_3H_3 + C_3H_3 \rightarrow$ A1	3.00E+36	–7.18	4234.0	Richter (2000); Slavinskaya and Frank (2009)
31	$C_4H_3 + C_2H_2$ = A1-	2.80E+03	2.90	5850	Frenklach *et al.* (1985); Frenklach and Warnatz (1987)
32	$C_4H_4 + C_2H_2$ = A1	4.47E+11	0.0	30010	Richter *et al.* (2005)
33	$C_3H_3 + OH = C_3H_2 + H_2O$	2.00E+13	0.0	23900.0	Miller and Bowman (1989)
34	$C_3H_3 + HO_2 = OH + CO + C_2H_3$	8.00E+11	0.0	23900.0	Davis *et al.* (1999)
35	$C_3H_3 + HO_2 = C_3H_4 + O_2$	3.00E+11	0.0	23900.0	Davis *et al.* (1999)
36	C_3H_3 + HCO = C_3H_4 + CO	2.50E+13	0.0	23900.0	Wang and Frenklach (1997)
Selected Reactions of C_5 Species					
37	$C_5H_5 + CH_3$ = A1 + 2H	1.00E+15	0.00	30000.0	Madden (1995)
38	$C_5H_5 + C_4H_2$ = Indenyl	1.20E+12	0.00	5030	Knjazev and Slagle (2002)
39	$C_5H_5 + C_4H_4$ = Indene + H	6.00E+11	0.00	5030	Knjazev and Slagle (2002)
40	$C_5H_5 + C_5H_5 \rightarrow$ A2 + 2H	4.30E+36	–6.268	45671.0	Shukla and Koshi (2011)
41	C_5H_5 + Benzyl → P2 + 2H	1.00E+15	0.00	1E+12	Granata *et al.* (2002)
42	$C_5H_6 + C_2H_3$ = A1 + CH_3	2.12E+20	–6.08	21310.0	Zhong (1997)
43	C_5H_6 + A1- = C_5H_5 + A1	3.10E+11	0.0	5500	Burcat and Dvinyaninov (1997)
44	$C_5H_6 + CH_3 = C_5H_5 + CH_4$	5.00E+11	0.0	5500	Bacskay and Mackie (2001)
Selected Reactions of C_6 Species					
45	A1- + $O_2 = C_6H_5O$ + O	2.09E+09	0.00	7463.9	Bittker (1991)
46	A1- + O = C_5H_5 + CO	9.00E+13	0.0	0.0	Tan and Frank (1996)
47	A1- + $C_2H_2 = C_8H_6$ + H	3.98E+13	0.00	10100.0	Granata *et al.* (2002)
48	A1- + C_3H_3 = Indene	1.00E+10	0.0	23900.0	Lindstedt (2002)
49	A1- + C_3H_3 = Indenyl + H	3.00E+12	0.0	23900.0	D'Anna (2000)
50	A1- + C_3H_4 = Indene + H	6.26E+09	2.61	56500	Zhang *et al.* (2010)
51	A1- + $C_4H_4 \rightarrow$ A2 + H	1.26E+04	2.610	1649.2	Shukla and Koshi (2011)
52	A1- + H = A1	5.71E+04	2.43	6273	Wang *et al.* (2007)
53	Al- + Al- = P2	2.00E+19	–2.05	2900	Wang and Frenklach (1997)
54	A1- + $C_8H_6 \rightarrow$ A3 + 2H	1.51E+35	–17.8	39600	Raj *et al.* (2012)
55	A1 + H = A1- + H_2	2.50E+14	0.0	16000	Wu *et al.* (2006)
56	A1 + OH = A1- + H_2O	1.60E+08	1.42	1450	Wu *et al.* (2006)
57	A1 + $CH_3 \rightarrow$ A1- + CH_4	4.42E+00	3.916	11463	Raj *et al.* (2012)
58	A1 + $C_3H_3 \rightarrow$ A1- + C_3H_4	2.27E+01	3.517	24065	Raj *et al.* (2012)
59	A1 + CH_3 = Toluene + H	5.67E+08	1.43	5650	Raj *et al.* (2012)
60	A1 + O = C_6H_5O + H	2.20E+13	0.0	4530	Baulch *et al.* (1992)
61	A1- + OH = C_6H_5OH	1.30E+13	0.0	10600	Baulch *et al.* (1992)
62	$C_6H_5O = CO + C_5H_5$	2.50E+11	0.0	43900	Lin and Lin(1986)
63	C_6H_5O + H = CO + C_5H_6	3.00E+13	0.0	23900.0	Wang and Frenklach (1997)
64	C_6H_5O + O → HCO + $2C_2H_2$ + CO	3.00E+13	0.0	23900.0	Wang and Frenklach (1997)
65	$C_6H_5OH + H = C_6H_5O + H_2$	1.15E+14	0.0	12400	He *et al.*(1986)
66	C_6H_5OH + O = C_6H_5O + OH	2.80E+13	0.0	7352	Emdee *et al.* (1992)
67	$C_6H_5OH + OH = C_6H_5O + H_2O$	6.00E+12	0.0	23900.0	He *et al.*(1986)
Selected Reactions of C_7 Species					
68	Benzyl + $CH_3 \rightarrow C_8H_{10}$	1.19E+13	0.00	221	Ergut *et al.* (2006)
69	Benzyl + H = A1- + CH_3	4.50E+35	–11.9	51860	Klippenstein *et al.* (2007)
70	Benzyl + C_2H_2 = Indene + H	6.00E+11	0.00	5030.0	Granata *et al.* (2002); Knjazev and Slagle (2002)
71	Benzyl + $C_3H_3 \rightarrow$ A2 + 2H	3.86E+12	0.00	6850.5	Kislov and Mebel (2007)
72	Benzyl = $C_5H_5 + C_2H_2$	3.00E+13	0.0	70000	Colket and Seery (1994)
73	Benzyl + H = Toluene	2.83E+35	–13.99	120613	Zhang *et al.* (2010)
74	Toluene = A1- + CH_3	2.16E+35	–20.61	144292	Zhang *et al.* (2010)
75	Toluene + H = Benzyl + H_2	6.47E+00	3.98	3394	Oehlschlaeger *et al.* (2006)
76	Toluene + H = A1 + CH_3	1.56E+13	0.0	5796	Baulch *et al.* (2005)
77	Toluene + CH_3 = Benzyl + CH_4	3.16E+11	0.0	9500.0	Wang *et al.* (2007)
Selected Reactions of C_8–C_9 Species					
78	C_8H_{10} + H → A1 + C_2H_5	1.20E+13	0.0	5100	Zhang and McKinnon (1995)

Table 4. *(continued).*

R#	Reactions	A	n	*Ea*	Ref.
79	Indene = Indenyl + H	1.73E+35	–15.2	116372	Blanquart *et al.* (2009)
80	Indenyl + C_3H_3=A2R5 + H_2	4.10E+15	–9.20	15153	Blanquart *et al.* (2009)
81	Indenyl + C_3H_2=A2R5 + H	1.00E+19	0.0	0.0	Zhang *et al.* (2010)
82	Indenyl + C_3H_3=P2- + H	3.00E+12	0.0	23900.0	D'Anna (2000)
83	Indenyl + C_3H_3=P2	4.00E+11	0.00	7000.0	Kislov and Mebel (2007); Dworkin *et al.* (2011)
84	Indenyl + C_5H_5=A3 + 2H	1.00E+13	0.00	8000.0	Marinov *et al.* (1998)
85	Indenyl + Benzyl → A4 + $2H_2$	2.00E+12	0.0	2000	Slavinskaya *et al.* (2005)
86	Indenyl + Indenyl → A4 + C_2H_2 + H_2	6.39E+29	–4.03	35205.5	Slavinskaya *et al.* (2005)
87	Indene + H = Indenyl + H_2	2.19E+08	1.77	3000.0	Marinov *et al.* (1998)
88	Indene + O = Indenyl + OH	1.81E+13	0.0	3080	Marinov *et al.* (1998)
89	Indene + OH = Indenyl + H_2O	3.43E+09	1.18	–447.0	Marinov *et al.* (1998)
90	Indene + CH_3 = Indenyl + CH_4	2.75E+00	3.614	3380.1	Raj *et al.* (2012)
91	Indene + C_3H_3 = A2R5 + H + H_2	1.50E+14	0.00	25912.2	Slavinskaya and Frank (2009)
92	Indene + C_3H_3 = P2 + H	1.54E+14	0.00	25912.2	Kislov and Mebel (2007); Dworkin *et al.* (2011)
Selected reactions of C_{10} Species					
93	1-Naphthyl + C_4H_4 → A3 + H	1.26E+04	2.610	1649.2	
94	1-Naphthyl + C_2H_2 = A2R5 + H	8.54E+22	–2.849	11370.0	Richter (2000); Granata *et al.* (2002)
95	1-Naphthyl + $A1^-$ = FLTHN + 2H	5.00E+12	0.00	0.0	Marinov *et al.*(1996)
96	1-Naphthyl + A1 = FLTHN + H_2 + H	4.00E+11	0.00	4000.0	Marinov *et al.* (1996)
97	1-Naphthyl + H = A2	1.00E+14	0.0	0.0	Marinov et al (1996)
98	A2 + O = 1-Naphthyl + OH	2.00E+13	0.0	7400	Dworkin *et al.* (2011)
99	A2 + H → 1-Naphthyl + H_2	1.15E+14	0.0	12400.0	Baulch *et al.* (1992)/1.3
100	A2 + OH = 1-Naphthyl + H_2O	2.10E+13	0.0	4600.0	Madronich and Felder (1985)
101	A2 + C_2H_3 = 1-Naphthyl + C_2H_4	5.00E+13	0.0	16000	Harris *et al.* (1988)
102	A2 + C_2H_2 = A2R5 + 2H	1.00E+19	0.00	2390.0	Frenklach *et al.* (1998); Celnik *et al.* (2007)
Selected Reactions of C_{11}–C_{14} Species					
103	P2 = P2- + H	9.00E+37	–6.63	119580	Wang and Frenklach (1997)
104	P2 + H = P2- + H_2	2.50E+14	0.0	16000	Wang and Frenklach (1997)
105	P2- + H2 → P2 + H	2.46E+04	2.486	3682.2	Raj *et al.* (2012)
106	P2 + OH = P2- + H_2O	1.60E+08	1.42	1450	Wang and Frenklach (1997)
107	P2 + CH_3 → P2- + CH_4	1.49E-01	4.002	11934.1	Raj *et al.* (2012)
108	P2- + CH_4 → P2 + CH_3	1.27E-02	4.309	5108.7	Raj *et al.* (2012)
109	P2- + C_2H_2 = A3 + H	2.60E+4	2.55	5644.4	Richter *et al.* (2000)
110	P2 + C_3H_3 → P2- + C_3H_4	3.32E+00	3.571	24292	Raj *et al.* (2012)
111	P2- + C_3H_4 → P2 + C_3H_3	3.60E-01	3.795	1619.8	Raj *et al.* (2012)
112	A2R5 + O → 1-Naphthyl + HCCO	2.00E+13	0.0	7400	Dworkin *et al.* (2011)
113	A3 → A2R5 + C_2H_2	3.29E+06	2.00	3161.1	Frenklach *et al.* (2005); Celnik *et al.* (2007)
114	A3 + O_2 → A2R5 + HCO + CO	2.10E+12	0.0	7470	Wang and Frenklach (1997)
115	A4 = C_4H_2 + A2R5	6.00E+02	2.23	–569.2	Wang and Frenklach (1997); Slavinskaya and Frank (2009); Dworkin *et al.* (2011)

Note: $K = AT^n \exp(-Ea/RT)$; A: $cm^3/mole/s$; *Ea*: cal/mole; p.w.: present work; Reactions with the" =" sign are reversible, and those with " → " are irreversible

Hence, even if some transient species were not identified, the application of a simplified comprehensive mechanism is appropriate for long-term environmental engineering practice. Thus, if only final Acpy emission levels are of interest, the proposed simplified model for calculating Acpy emissions from restaurant cooking activities offers an excellent alternative to time-consuming and computationally expensive comprehensive mechanisms.

Temperature Profiles

Figs. 5(a) and 5(b) show a comparison of 2 curves. The averaged levels of temperature varied in the vertical direction (Y-axis). The curve in Fig. 5(a) represents the averaged levels of temperature variation at different positions on the Y-axis (in the XY-plane), 7.35 cm from the torch position. The curve in Fig. 5(b) represents the average temperature variation at a position 37.35 cm from the torch (in the XY plane). These simulation results show that the variation trend of the curve at 7.35 cm is considerably greater than that of the curve at 37.35 cm.

When inputting plasma power at 24 A (Fig. 6), the highest temperature area in the flow field is in the central position of the plasma torch, where the simulated temperature reaches 2243 K. Fig. 6(a) shows the temperature distribution in the x direction (horizontal plane) from x = –2.0 cm (left of the torch) to x = +37.5 cm (right of the torch) after 0.1 s

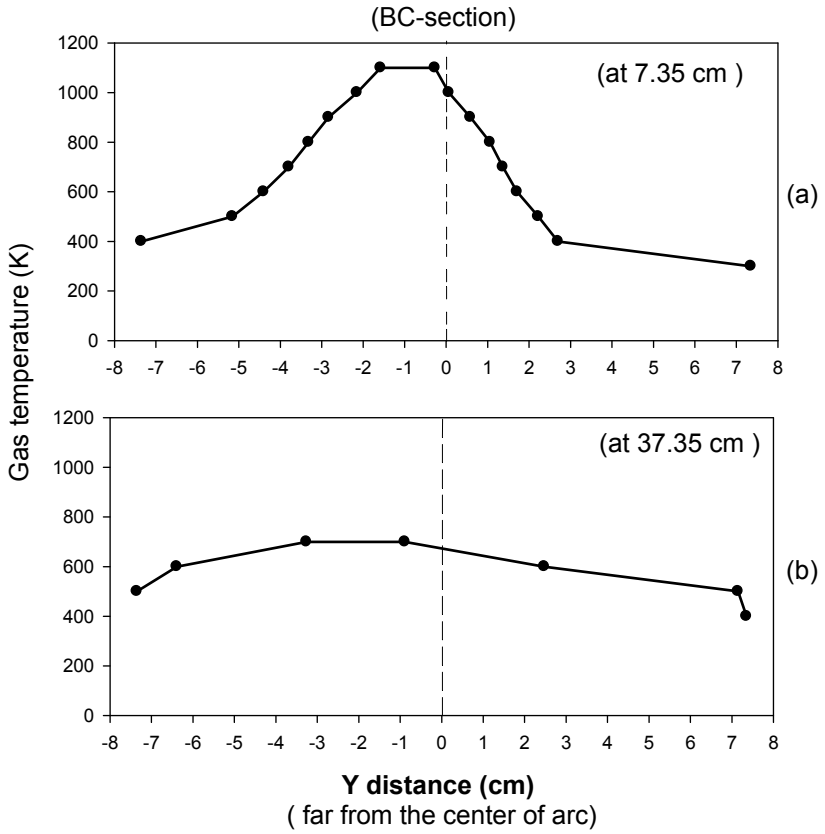

Fig. 5. The simulated gas temperatures at different Y distances far from the center of plasma torch paralleled the BC-section at X= 7.35 cm (a) and X= 37.35 cm (b).

simulation. The temperature distribution varies in the plasma torch zone, which can be explained by the efficient turbulent heat transfer of the torch. Similarly, there is no significant temperature gradient in the bulk zone away from the position of x = +18 cm. Moreover, low-temperature zones (less than 400 K) exist in the upper region of the duct, where temperatures are the lowest and no gradients exist. This can be explained by the effect of the less turbulent flow in this part of the duct and by the cooling wall temperature on the steel duct boundary. The temperature difference between the center zone of the torch and near the wall of the boundary zones is approximately 2000 K. On a practical scale, the temperature gradient between the bulk and the boundary zone might be expected to be accepted in this study. Figs. 6(b) and 6(c) show the temperature profiles in the vertical plane at 7.35 cm and 37.35 cm after 0.1 s numerical simulation, respectively. The upper bulk region has a uniform temperature profile with no temperature gradients. Because of diffusion, the temperature of the hottest mixture fractions decreases when the X-distance from the center of the plasma torch increases. After 0.1 s, mixtures nearing stoichiometry reach the steady stage (after finishing the main decomposition of Acpy) at X = 7.35 cm, whereas these mixtures are in the low torch regime on the left side of the profile (at positions from Y = –7 to Y = –1 cm) at X = 3.75 cm (Fig. 6(b)). The most reactive mixture fraction is not the center of the torch area (i.e., the chemical reactions involved are supposed to be the most active). However, the temperature gradient within the plasma torch zone is larger than that of the post-torch zone. Temperature differences of approximately 600 K and 350 K appear between the torch area and temperature near the upper areas at 7.35 cm and 37.35 cm, respectively. This is the result of air stream shifting from the torch nozzle.

Concentration Profiles

The accuracy of CFD simulations depends on many factors. For example, the effects of appropriate geometry boundaries, the inlet turbulence parameters, and the selected turbulence models (such as the low-Reynolds number k-ε model, renormalization group k-ε model, or Shear Stress Transport k-w model) are important (Rong *et al.*, 2011). Based on the characteristics of a plasma torch, particular attention should be paid to the boundaries chosen for the plasma-reaction domain. This is because both the position of the domain boundaries and the type of condition imposed (e.g., pressure node, velocity node, and non-reflecting surface) have significant effects on the results of modal analysis. These limits are likely to be the same limits of the computational domain in the CFD simulation, which is performed in the successive steps of the decomposition of acenaphthylene compound in the APR. The contour plots in Fig. 7 show the predicted levels of mass fraction of Acpy, with the progress variable on the horizontal axis (x-direction) or the vertical symmetry plane near the plasma torch.

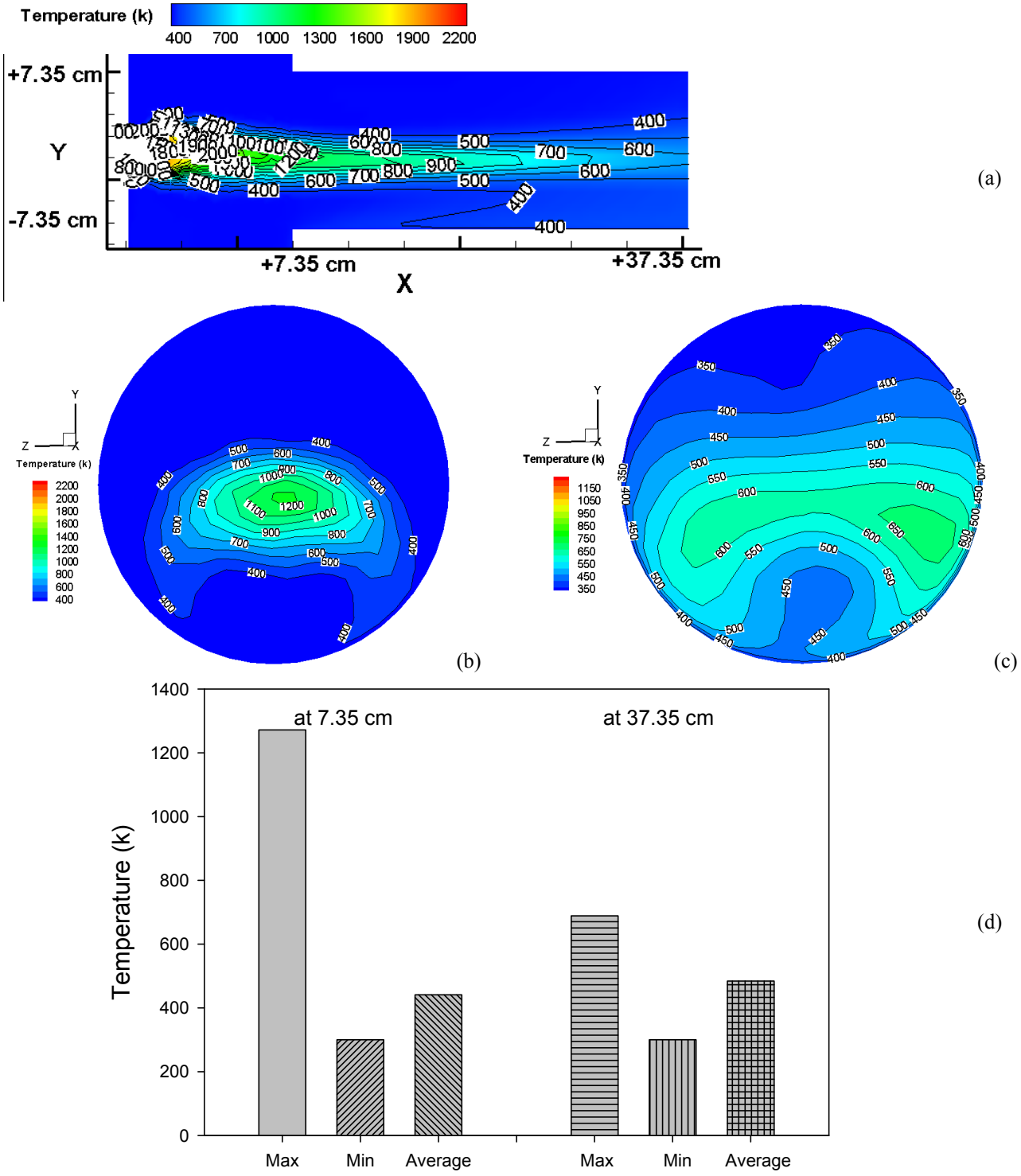

Fig. 6. Temperature profiles (K): (a) at different X distances far from the center of plasma torch; (b–c) the distribution profile paralleled the BC-section at X= 7.35 (b) and X= 37.35 cm (c); (d) comparison of temperature levels between at X= 7.35 and X= 37.35 cm.

- ***Acpy ($C_{12}H_8$)***

In the plasma-torch zone (i.e., the ABCD-box in Fig. 4), temperature distribution gradients affect the concentration of Acpy profiles within a cross-section of the duct. High thermal energy is the dominant factor in the decomposition process, affecting both the gas kinetics and the final product performance. A comparison of temperature distribution shows that higher temperatures yield greater removal efficiency. Fig. 7 shows the concentration profile of Acpy (mass fraction %) within the reactor. After calculation, the residence time of reaction is approximately 0.12 s. According to this profile, Acpy was decomposed and destructed

through the reaction zone of the plasma torch. In general, when the distance in the X direction increases (i.e., moving away from the plasma torch), the concentration of the reactant mixture decreases. This phenomenon is due to the transport of temperature and reactive species from hottest mixtures to coldest mixtures, which increases with the dissipation of high energy.

We sampled and measured the concentration of Acpy in the inlet of the duct at 2.18×10^{-9} (mass fraction %). Based on this feeding level, the simulated concentration of Acpy

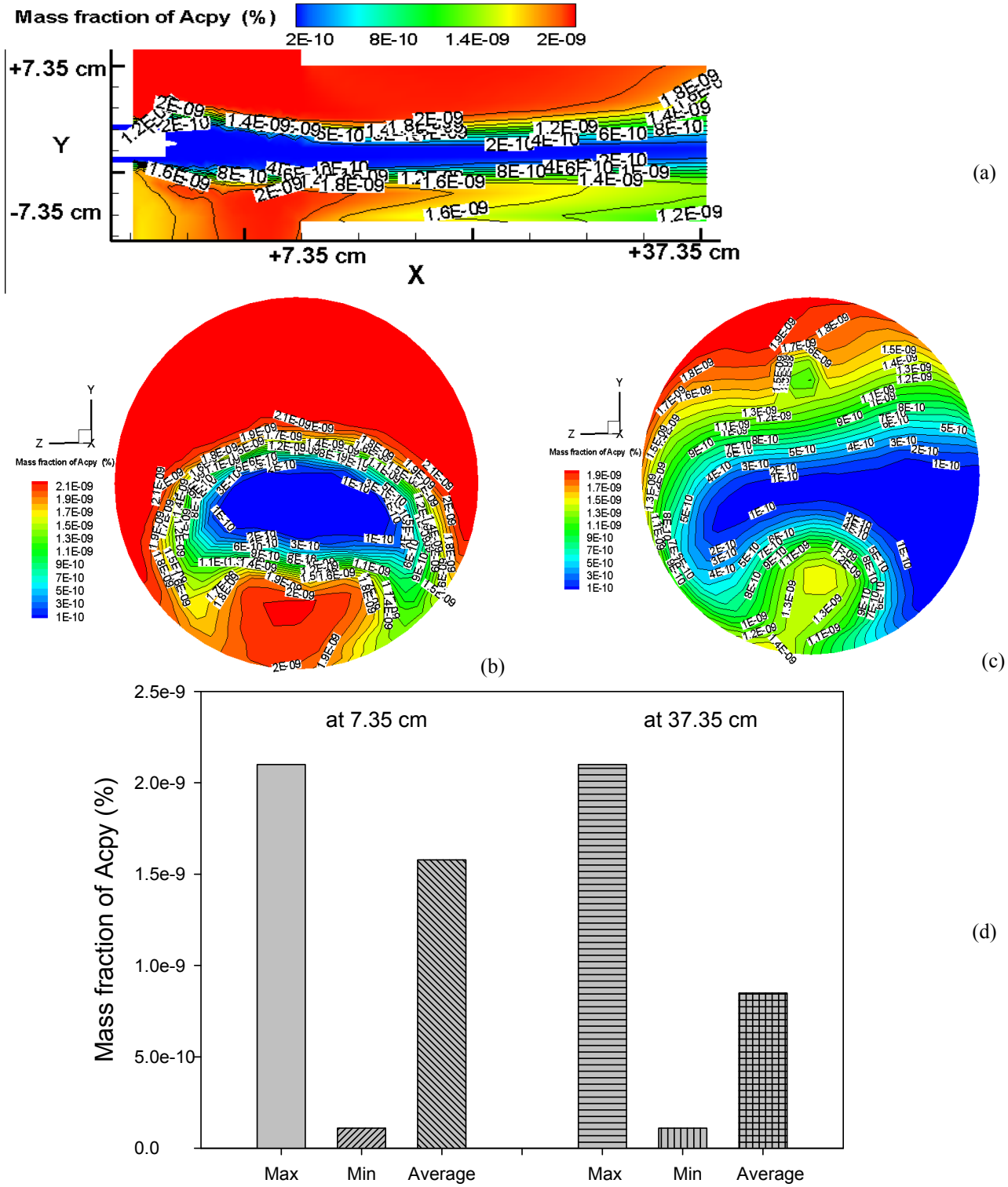

Fig. 7. Concentration of Acpy profiles (%): (a) at different X distances far from the center of plasma torch; (b–c) the distribution profile paralleled the BC-section at X= 7.35 (b) and X= 37.35 cm (c); (d) comparison of $C_{12}H_8$ levels between at X= 7.35 and X= 37.35 cm.

in the duct ranged from 8.49×10^{-10} to 1.5×10^{-9} (mass fraction %), and the simulated removal efficiencies of Acpy ranged from 31.1% to 61.05%, respectively. Comparing the average simulated removal efficiency (approximately 61.05%) of Acpy to the actual experimental data (averaging approximately 65.2%) measured in the reactor shows that the CFD simulations slightly underestimated removal efficiency. Furthermore, faster mixing and a higher local temperature characterize the decomposed configuration the correlation of both temperature and velocity related to the lower section at X = 7.35 cm (as shown in Figs. 6(b) and 7(b)) showed that the removal decomposition efficiency might differ only slightly from Y = –7.35 to + 7.35 cm (as Fig. 7(b) shows) because the plasma torch had a small injection angle (less than 5°).

Reaction Pathway

Fig. 8 shows the simplified pathways of Acenaphthylene decomposition and formation. These species include benzene (A1, C_6H_6), toluene (C_7H_8), indene (C_9H_8), naphthalene (A2, $C_{10}H_8$), biphenyl, (P2, $C_{12}H_{10}$), acenaphthylene (A2R5, $C_{12}H_8$), phenanthrene (A3, $C_{14}H_{10}$), pyrene (A4, $C_{16}H_{10}$), and some of their branched structures and radicals. In the plasma reactor, the major pathways for acenaphthylene decomposition include Indenyl + C_3H_3 = A_2R_5 + H_2 (R#80), Indenyl + C3H2 = A2R5 + H (R#81), Indene + C_3H_3 = A2R5 + H + H_2 (R#91), 1-Naphthyl + C_2H_2 = A2R5 + H (R#94), A2 + C_2H_2 = A2R5 + 2H (R#102), A2R5 + O → 1-Naphthyl + HCCO (R#112), and A4 = C_4H_2 + A2R5 (R#115). The major pathways for acenaphthylene formation include A3 → A2R5 + C_2H_2 (R#113) and A3 + O_2 → A2R5 + HCO + CO (R#114). The above reactions have been included with the thermochemistry of the relevant species as shown in Table 4.

For flame temperatures < 1550 K, the key reaction for one ring molecule formation is $H_2CCCH + C_2H_2 = C_5H_5$. At this temperature, the propargyl radical reacts with C_2H_2 to produce C_5H_5 (Slavinskaya and Frank, 2009). Cyclopentadienyl further forms A1 by reacting with methyl radicals in the main reaction zone and in the post-flame zone. Zhong and Bozzelli (1997) proposed a submechanism of important cyclopentadienyl (C_5H_6) radical reactions and tested it in an elementary model for benzene combustion.

- ***C_6 Mechanism***

The common pathways considered in most mechanisms involve propargyl (C_3H_3) recombination and the addition of C_2Hx on C_4Hy molecules (Zhang *et al.*, 2009). Benzene is primarily produced by propargyl (C_3H_3) recombination (R#30) (Wang and Frenklach, 1997). Sharma and Green (2009) studied a new pathway (R#31) for the formation of benzene through the addition of CH_3 on cyclopentadienyl (C_5H_5) radicals (Sharma and Green, 2009). The most important steps involved in this PAH formation process require phenyl (C_6H_5) and naphthyl ($C_{10}H_7$) to be oxidized by O_2 (Marinov *et al.*, 1998). Ethynylbenzene (C_8H_6) is a key component in the subsequent growth of PAH. The hydrogen abstraction/acetylene addition (HACA) mechanism, through the phenyl radical (C_6H_5) addition to acetylene, is the main route to form ethynylbenzene (C_8H_6). This reaction pathway explains more than 75% of benzene depletion. Ethynylbenzene is also formed (approximately 20%–25%) by the addition of the C_4H_5 radical to C_4H_2 (Granata *et al.*, 2002).

- ***C_7–C_9 Mechanism***

The radicals H and CH_3 formed from the reactions R#76 and R#77 can attack toluene, accelerating the consumption of toluene. During the benzene decomposition period (R#84, R#85), a pathway beginning with the formation of biphenyl is followed by the sequential addition of acetylene, first to Phenanthrene ($C_{14}H_{10}$), and then to Pyrene (Richter and Howard, 2000).

- ***C_{10} Mechanism***

One of the important pathways (R#40) for the formation of naphthalene is through the self-combination of cyclopentadienyl radicals (C_5H_5) (Dean, 1990; Kislov and Mebel, 2007). The key step in the naphthalene production process is phenyl oxidation by O_2. This step produces a phenoxy radical that decomposes to cC_5H_5 + CO. The cyclopentadienyl radicals self-combine and then undergo H-atom shifts and 2 H-atom ejections, leading to naphthalene production (Marinov *et al.*, 1998). The reaction (R#94) of 1-naphthyl with acetylene produces acenaphthylene (A2R5, $C_{12}H_8$) (Richter *et al.*, 1999).

- ***C_{11}–C_{14} Mechanism***

The formation of fluoranthene (FLTHN, $C_{16}H_{10}$) (R#95, R#96), a key species for fullerene formation, begins with 1-naphthyl reacting with benzene or phenyl (Marinov *et al.*, 1996). Phenanthrene (A3, $C_{14}H_{10}$) (R#109), a key species for further PAH growth, is primarily formed by the reaction of C_2H_2 with biphenyl radicals (Wang and Frenklach, 1997). Acenaphthylene ($C_{12}H_8$) was consistently under-predicted by a factor of 10 throughout the n-butane flame when using $C_{10}H_7 + C_2H_2$ = Acenaphthylene + H as the Acenaphthylene formation step.

A reactive model based on CFD code must be just detailed enough to predict the effects of Acpy oxidation on the flow field. Thus, more computational resources can be dedicated to simulating the dynamics of flow, the concentration of the main species, and the heat and radioactive exchange.

The experiments and CFD comparisons in this study show satisfactory agreement on Acpy removal efficiency, especially in the horizontal axis (x-direction). However, adding more reaction mechanisms to the simulation may be necessary to accommodate the combustion reactions of complex PAHs in a plasma reactor.

CONCLUDING REMARKS

This study presents numerical simulations of decomposing acenaphthylene in an atmospheric plasma reactor to treat cooking fumes. We also compared experimental results with the simulation data. The online measured temperature levels in the exhaust of the reactor ranged from 350 to 600 K, which is similar to the simulation levels. The simulation

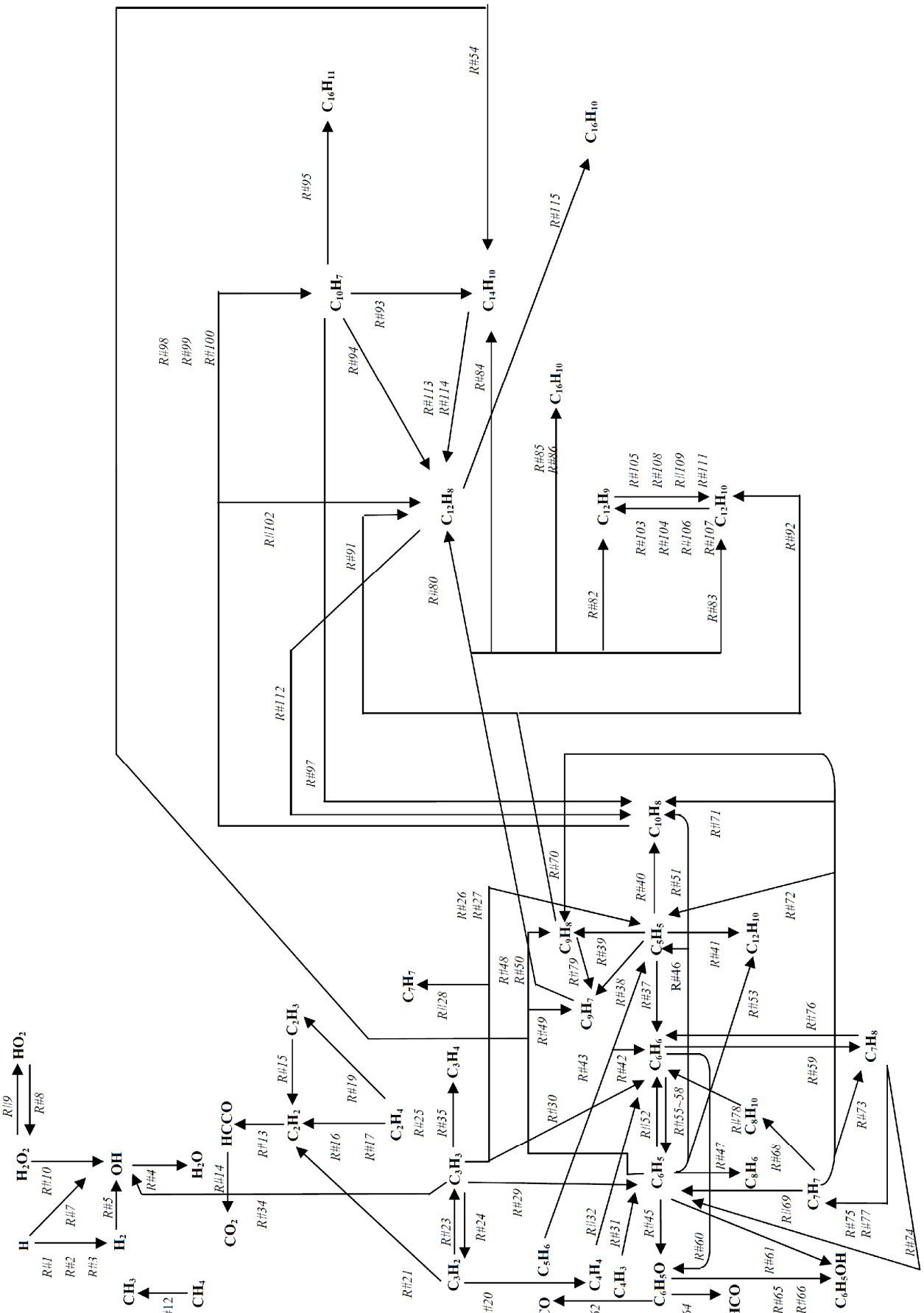

Fig. 8. Simplified pathway of Acenaphthylene decomposition.

results slightly underestimated Acpy removal efficiency compared to the experimental data. Actual measurements of acenaphthylene decomposition indicate that the maximum relative error of calculations is less than 6.3%. These results show that the CFD method is a useful tool in the rational design of an atmospheric plasma reactor to treat cooking fumes.

ACKNOWLEDGMENTS

The authors would like to thank the National Science Council of the Republic of China, Taiwan for financially supporting this research under Contract No. NSC95-2221-E020-021.

REFERENCES

ATSDR (Agency for Toxic Substances and Disease Registry) (1990). Toxicological Profile for Polycyclic Aromatic Hydrocarbons. Acenaphthene, Acenaphthylene, Anthracene, Benzo(a)anthracene, Benzo(a)pyrene, Benzo(b)fluoranthene, Benzo(g,i,h)perylene, Benzo(k)fluoranthene, Chrysene, Dibenzo(a,h)anthracene, Fluoranthene, Fluorene, Indeno(1,2,3-c,d)pyrene, Phenanthrene, Pyrene. Prepared by Clement International Corporation, under Contract No. 205-88-0608. ATSDR/TP-90-20.

Bacskay, G.B. and Mackie, J.C. (2001). The Pyrolysis of Cyclopentadiene: Quantum Chemical and Kinetic Modelling Studies of the Acetylene Plus Propyne/Allene Decomposition Channels. *Phys. Chem. Chem. Phys.* 3: 2467–2473.

Bari, Md. A., Baumbach, G., Kuch, B. and Scheffknecht, G. (2011). Air Pollution in Residential Areas from Wood-fired Heating. *Aerosol Air Qual. Res.* 11: 749–757.

Baulch, D.L., Cobos, C.J., Cox, R.A., Esser, C., Frank, P., Just, T., Kerr, J.A., Pilling, M.J., Troe, J., Walker, R.W., and Warnatz, J. (1992). Evaluated Kinetic Data for Combustion Modelling. *J. Phys. Chem. Ref. Data* 21: 411–734.

Baulch, D.L., Cobos, C.J., Cox, R.A., Frank, P, Hayman, G., Just, Th., Kerr, J.A., Murrells, T., Pilling, M.J., Troe, J., Walker, R.W. and Warnatz, J. (1994). Evaluated Kinetic Data for Combustion Modelling. Supplement I. *J. Phys. Chem. Ref. Data* 23: 847–1033.

Baulch, D.L., Bowman, C.T., Cobos, C.J., Cox, R.A., Just, Th., Kerr, J.A., Pilling, M.J., Stocker, D., Troe, J., Tsang, W., Walker, R.W. and Warnatz, J. (2005). Evaluated Kinetic Data for Combustion Modeling: Supplement II. *J. Phys. Chem. Ref. Data* 34: 757–1397.

Blanquart, G., Pepiot-Desjardins, P. and Pitsch, H. (2009). Chemical Mechanism for High Temperature Combustion of Engine Relevant Fuels with Emphasis on Soot Precursors. *Combust. Flame* 156: 588–607.

Burcat, A. and Dvinyaninov, M. (1997). Detailed Kinetics of Cyclopentadiene Decomposition Studied in a Shock Tube. *Int. J. Chem. Kinet.* 29: 505–514.

Celnik, M.S., Raj, A., West, R.H., Patterson, R.I.A. and Kraft, M. (2007). An Aromatic Site Description of Soot Particles, Technical Report 51, c4e-Preprint Series, Cambridge, Available at: http://como.cheng.cam.ac.uk/index.php?Page=News&ID=00000000026.

Chang, H.C., Mi, H.H., Lin, Y.C., Hsieh, L.T. and Chao, H.R. (2011). Removal of Gaseous Polycyclic Aromatic Hydrocarbons from Cooking Fumes Using an Atmospheric Plasma Reactor. *J. Environ. Sci. Health., Part A* 46: 1443–1449.

Colket, M.B. and Seery, D.J. (1994). Reaction Mechanisms for Toluene Pyrolysis. *Proc. Combust. Inst.* 25: 883–891.

D'Anna, A., Violi, A. and D'Alessio, A. (2000). Modeling the Rich Combustion of Aliphatic Hydrocarbons. *Combust. Flame* 121: 418–429.

Dagaut, P., Pengloan, G. and Ristori, A. (2002). Oxidation, Ignition and Combustion of Toluene: Experimental and Detailed Chemical Kinetic Modelling. *Phys. Chem. Chem. Phys.* 4: 1846–1854.

Dean, A.M. (1990). Detailed Kinetic Modeling of Autocatalysis in Methane Pyrolysis. *J. Phys. Chem.* 94: 1432–1439

Dworkin, S.B., Zhang, Q., Thomson, M.J., Slavinskaya, N.A. and Riedel, U. (2011). Application of an Enhanced PAH Growth Model to Soot Formation in a Laminar Coflow Ethylene/Air Diffusion Flame. *Combust. Flame* 158: 1682–1695.

Emdee, J.L., Brezinsky, K. and Glassman, I. (1992). A Kinetic Model for the Oxidation of Toluene Near 1200 K. *J. Phys. Chem.* 96: 2151–2161.

Ergut, A. Granata, S. Jordan, J, Carlson, J. Howard, J.B. Richter, H. and Levendis, Y.A. (2006). PAH Formation in One-Dimensional Premixed Fuel-Rich Atmospheric Pressure Ethylbenzene and Ethyl Alcohol Flames. *Combust. Flame* 144: 757–772.

Frenklach, M., Clary, D.W., Gardiner, W.C. Jr, and Stein, S.E. (1985). Detailed Kinetic Modeling of Soot Formation in Shock-Tube Pyrolysis of Acetylene. *Proc. Combust. Inst.* 20: 887–901.

Frenklach, M. and Warnatz, J. (1987). Detailed Modeling of PAH Profiles in a Sooting Low-Pressure Acetylene Flame. *Combust. Sci. Technol.* 51: 265–283.

Frenklach, M., Moriarty, N.W. and Brown, N.J. (1998). Hydrogen Migration in Polyaromatic Growth. *Symp. (Int.) Combust.* 27: 1655–1661.

Frenklach, M. Schuetz, C.A. and Ping, J. (2005). Migration Mechanism of Aromatic-Edge Growth. *Proc. Combust. Inst.* 30: 1389–1396.

GAMBIT, Inc. (2007). GAMBIT 2.4 User's Guide.

Granata, S., Faravelli, T., Ranzi, E., Olten, N. and Senkan, S. (2002). Kinetic Modeling of Counterflow Diffusion Flames of Butadiene. *Combust. Flame* 131, 273–284.

Harris, S.J., Weiner, A.M. and Blint, R.J. (1988). Formation of Small Aromatic Molecules in a Sooting Ethylene Flame. *Combust. Flame* 72: 91–109.

He, Y.Z., Mallard, W.G. and Tsang, W. (1988). Kinetics of Hydrogen and Hydroxyl Radical Attack on Phenol at High Temperatures. *J. Phys. Chem.* 92: 2196–2201.

Hsieh, L.T., Lee, W.J., Chen, C.Y., Wu, Y.P., Chen, S.J. and Wang, Y.F. (1998). Decomposition of Methyl Chloride by Using an RF Plasma Reactor. *J. Hazard. Mater.* 63:

69–90.

Hsieh, L.T. (2007). Treatment of Cooking Oil Exhausts by the Application of Combining Atmospheric Plasma Technology and Enzyme Scrubbing, Contract No. NSC95-2221-E020-021, National Science Council of the Republic of China, Taiwan.

Isaacson, A.D. (1997). Harmonic and Anharmonic Rate Constants and Transmission Coefficients Obtained from Ab Initio Data. *J. Phys. Chem.* 107: 3832–3839.

Karkach, S.P. and Osherov, V.I. (1999). Ab Initio Analysis of the Transition States on the Lowest Triplet H_2O_2 Potential Surface. *J. Phys. Chem.* 110: 11918–11927.

Kiefer, J.H., Mizerka, L.J., Patel, M.R. and Wei, H.C. (1985). A Shock Tube Investigation of Major Pathways in the High-Temperature Pyrolysis of Benzene. *J. Phys. Chem.* 89: 2013–2019.

Kim, C., Noh, K.C. and Hwang, J. (2010). Numerical Investigation of Corona Plasma Region in Negative Wire-to-duct Corona Discharge. *Aerosol Air Qual. Res.* 10: 446–455.

Kislov, V.V. and Mebel, A.M. (2007). The Formation of Naphthalene, Azulene, and Fulvalene from Cyclic C_5 Species in Combustion: An Ab Initio/RRKM Study of 9-H-Fulvalenyl (C_5H_5-C_5H_4) Radical Rearrangements. *J. Phys. Chem. A*. 111: 9532–9543.

Klippenstein, S.J., Harding, L.B. and Georgievskii, Y. (2007). On the Formation and Decomposition of C_7H_8. *Proc. Combust. Inst.* 31: 221–229.

Knjazev, V.D. and Slagle, I.R. (2002). Kinetics of the Reaction between Propargyl Radical and Acetylene. *J. Phys. Chem. A.*, 106: 5613–5617.

Knobloch, K., Szedzikowski, S. and Slusarcyk-Zablobona, A. (1969). Acute and Subacute Toxicity of Acenaphthene and Acenaphthylene. *Med. Pracy.* 20: 210–222.

Lai, S.C., Ho, K.F., Zhang, Y.Y., Lee, S.C., Huang, Y. and Zou, S.C. (2010). Characteristics of Residential Indoor Carbonaceous Aerosols: A Case Study in Guangzhou, Pearl River Delta Region. *Aerosol Air Qual. Res.* 10: 472–478.

Li, C.T., Lin, Y.C., Lee, W.J. and Tsai, P.J. (2003). Emission of Polycyclic Aromatic Hydrocarbons and Their Carcinogenic Potencies from Cooking Sources to the Urban Atmosphere. *Environ. Health Perspect.* 111: 483–487.

Lin, C.Y. and Lin, M.C. (1986). Thermal Decomposition of Methyl Phenyl Ether in Shock Waves: the Kinetics of Phenoxy Radical Reactions. *J. Phys. Chem.* 90: 425–431.

Lindstedt, R.P. and Rizos, J.A. (2002). The Formation and Oxidation of Aromatics in Cyclopentene and Methyl-Cyclopentadiene Mixtures. *Proc. Combust. Inst.* 29: 2291–2298

Liu, S.H., Lin, Y.C. and Hsu, K.H. (2012). Emissions of Regulated Pollutants and PAHs from Waste-cooking-oil Biodiesel-fuelled Heavy-duty Diesel Engine with Catalyzer. *Aerosol Air Qual. Res.* 12: 218–227.

Madronich, S. and Felder, W. (1985). Kinetics and Mechanism of the Reaction of Hydroxyl with Benzene. *J. Phys. Chem*. 89: 3556–3561.

Magureanu, M., Piroi, D., Mandache, N.B., David, V., Medvedovici, A. and Parvulescu, V.I. (2010). Degradation of Pharmaceutical Compound Pentoxifylline in Water by Non-Thermal Plasma Treatment. *Water Res*. 44: 3445–3453.

Marinov, N.M., Pitz, W.J., Westbrook, C.K., Castaldi, M.J. and Senkan, S.M. (1996). Modeling of Aromatic and Polycyclic Aromatic Hydrocarbon Formation in Premixed Methane and Ethane Flames. *Combust. Sci. Technol.* 116–117:211–287.

Marinov, N.M., William, J.P. and Westbrook, C.K. (1998). Aromatic and Polycyclic Aromatic Hydrocarbon Formation in a Laminar Premixed n-Butane Flame. *Combust. Flame* 114: 192–213.

Masih, J., Singhvi, R., Kumar,K., Jain, V.K. and Taneja, A. (2012). Seasonal Variation and Sources of Polycyclic Aromatic Hydrocarbons (PAHs) in Indoor and Outdoor Air in a Semi Arid Tract of Northern India. *Aerosol Air Qual. Res.* 12: 515–525.

Miller, J.A. and Bowman, C.T. (1989). Mechanism and Modeling of Nitrogen Chemistry in Combustion. *Prog. Energy Combust. Sci.* 15: 287–338.

Miller, J.A. and Klippenstein, S.J. (2003). The Recombination of Propargyl Radicals and other Reactions on a C_6H_6 Potential. *J. Phys. Chem. A.* 107: 7783–7799.

Miltner, M., Miltner, A., Harasek, M. and Friedl, A. (2007). Process Simulation and CFD Calculations for the Development of an Innovative Baled Biomass-Fired Combustion Chamber. *Appl. Therm. Eng.* 27: 1138–1143.

Moustakasa, K., Fattab, D., Malamisa, S., Haralambousa, K. and Loizidoua, M. (2005). Demonstration Plasma Gasification/Vitrification System for Effective Hazardous Waste Treatment. *J. Hazard. Mater.* 123: 120–126.

Oehlschlaeger, M.A., Davidson, D.F. and Hanson, R.K. (2006). Experimental Investigation of Toluene + H → Benzyl + H_2 at High Temperatures. *J. Phys. Chem. A.* 110: 9867–9873.

Panagopoulos, I., Karayannis, A., Kassomenos, P. and Aravossis, K. (2011). A CFD Simulation Study of VOC and Formaldehyde Indoor Air Pollution Dispersion in an Apartment as Part of an Indoor Pollution Management Plan. *Aerosol Air Qual. Res.* 11: 758–762.

Raj, A., Prada, I.D.C., Amer, A.A. and Chung, S.H. (2012). A Reaction Mechanism for Gasoline Surrogate Fuels for Large Polycyclic Aromatic Hydrocarbons. *Combust. Flame* 159: 500–515.

Richter, H. and Howard, J.B. (2000). Formation of Polycyclic Aromatic Hydrocarbons and Their Growth to Soot—A Review of Chemical Reaction Pathways. *Prog. Energy Combust. Sci.* 26: 565–608.

Richter, H., Granata, S., Green, W.H. and Howard, J.B. (2005). Detailed Modeling of PAH and Soot Formation in a Laminar Premixed Benzene/Oxygen/Argon Low-Pressure Flame. *Proc. Combust. Inst.* 30: 1397–1405.

Rong, L., Elhadidi, B., Khalifa, H.E., Nielsen, P.V. and Zhang, G. (2011). Validation of CFD Simulation for Ammonia Emissions from an Aqueous Solution. *Comput. Electron. Agric.* 75: 261–271.

Rotenberg, I.S. and Mashbits, F.D. (1965). Toxicological Aspects of Acenaphthylene. *Gig. Tr. Prof. Zabol.* 9: 53–

54. (Cited in U.S. EPA, 1987)
Sharma, S. and Green, W.H. (2009). Computed Rate Coefficients and Product Yields for c-C_5H_5 + CH_3 f Products. *J. Phys. Chem. A* 113: 8871–8882.
Shatalov, O.P., Ibraguimova, L.B., Pavlov, V.A., Smekhov, G.D. and Tunik, Y.V. (2009). Analysis of the Kinetic Data Described Oxygen-Hydrogen Mixtures Combustion, Proc. 4th European Combustion Meeting, Vienna, Austria.
Shukla, B. and Koshi, M. (2011). Comparative Study on the Growth Mechanisms of PAHs. *Combust. Flame* 158: 369–375.
Slavinskaya, N.A., Braun-Unkoff, M. and Frank, P. (2005). Modelling of PAH and Polyyne Formation in Premixed Atmospheric Flames C_2H_4/Air, Proc. 2th European Combustion Meeting, Louvain-la-Neuve, Belgien.
Slavinskaya, N.A. and Frank, P. (2009). A Modelling Study of Aromatic Soot Precursors Formation in Laminar Methane and Ethene Flames. *Combust. Flame* 156: 1705–1722.
Smith, G.P., Golden, D.M., Frenklach, F., Moriarty, N.W., Eiteneer, B., Goldenberg, M., Bowman, C.T., Hanson, R.K., Song, S., Gardiner, W.C.J., Lissianski, V.V. and Qin, Z. (1999). GRI-Mech 3.0, Available at: http://www.me.berkeley.edu/gri-mech/.
Tan, Y. and Frank, P. (1996). A Detailed Comprehensive Kinetic Model for Benene Oxidation Using the Recent Kinetic Results, Proc. 26th Symposium (International) on Combustion, Napoli, Italy, 26: 677–684.
Tsai, J.H., Huang, K.L., Chiu, C.C., Lin, C.C., Kuo, W.C., Lin, W.Y., Chaung, H.C., Yang, T.H. and Chen, S.J. (2011). Particle-bound PAHs and Particle-extract-induced Cytotoxicity of Emission from a Diesel-generator Fuelled with Soy-biodiesel. *Aerosol Air Qual. Res.* 11: 822–836.
U.S. EPA (U.S. Environmental Protection Agency) (1989). Mouse Oral Subchronic Toxicity Study with Acenaphthylene, Prepared by Hazleton Laboratories, Inc., for the Office of Solid Waste, Washington, DC, Study No. 2390-129.
U.S. EPA (U.S. Environmental Protection Agency) (1990). Priority Pollutants, Available at: http://www.epa.gov/region1/npdes/permits/generic/prioritypollutants.pdf.
U.S. EPA (U.S. Environmental Protection Agency) (1991). Drinking Water Criteria Document for Polycyclic Aromatic Hydrocarbons (PAH). Prepared by the Environmental Criteria and Assessment Office, Office of Health and Environmental Assessment, U.S. Environmental Protection Agency, Cincinnati, OH, for the Office of Drinking Water, ECAO-CIN-D010.
Wang, H. and Frenklach, M. (1997). A Detailed Kinetic Modeling Study of Aromatics Formation in Laminar Premixed Acetylene and Ethylene Flames. *Combust. Flame* 110: 173–221.
Wu, J., Song, K.H., Litzinger, T., Lee, S.Y., Santoro, R., Linevsky, M., Colket, M. and Liscinsky, D. (2006). Reduction of PAH and Soot in Premixed Ethylene–Air Flames by Addition of Ethanol. *Combust. Flame* 144: 675–687.
Wang, H., You, X., Joshi, A.V., Davis, S.G., Laskin, A., Egolfopoulos, F. and Law, C.K. (2007). High-Temperature Combustion Reaction Model of H2/CO/C_1-C_4 Compounds, Available at: http://ignis.usc.edu/USC_Mech_II.htm.
Wu, T.S., Hsieh, L.T., Lin, S.L., Chang, Y.C., Chen, C.B. and Hung, C.H. (2010). Emissions from Using Viscous Agent-Treated Fishing Boat Fuel Oil: Tests with a Heavy-Duty Diesel Engine (HDDE) Dynamometer. *Aerosol Air Qual. Res.* 10: 76–85.
Yang, H.H., Lee, W.J., Chen, S.J. and Lai, S.O. (1998). PAH Emission from Various Industrial Stacks. *J. Hazard. Mater*. 60: 159–174.
Zhang, H.R., Eddings, E.G., Sarofim, A.F. and Westbrook, C.K. (2009). Fuel Dependence of Benzene Pathways. *Proc. Combust. Inst.* 32:377–385.
Zhang, H.Y. and McKinnon, J.T. (1995). Elementary Reaction Modeling of High-Temperature Benzene Combustion. *Combust. Sci. Technol*. 107: 261–300.
Zhang, L., Cai, J., Zhang, T. and Qi, F, (2010). Kinetic Modeling Study of Toluene Pyrolysis at Low Pressure. *Combust. Flame* 157: 1686–1697.
Zhong, X. and Bozzelli, J.W. (1997). Thermochemical and Kinetic Analysis on the Addition Reactions of H, O, OH, and HO_2 with 1,3 Cyclopentadiene. *Int. J. Chem. Kinet.* 29: 893–913.

Received for review, July 11, 2012
Accepted, September 10, 2012